Plasma measurements in a 100 W cylindrical Hall thruster

A. Smirnov,[a] Y. Raitses, and N. J. Fisch
Princeton University Plasma Physics Laboratory, P.O. Box 451, Princeton, New Jersey 08543

(Received 31 July 2003; accepted 30 November 2003)

Conventional annular Hall thrusters become inefficient when scaled to low power. Their lifetime decreases significantly due to the channel wall erosion. Cylindrical Hall thrusters, which have lower surface-to-volume ratio and, thus, seem to be more promising for scaling down, exhibit performance comparable with conventional annular Hall thrusters of the similar size. Plasma potential, ion density, and electron temperature profiles were measured inside the 2.6 cm cylindrical Hall thruster with the use of stationary and slow movable emissive and biased Langmuir probes. Potential drop in the 2.6 cm cylindrical Hall thruster is localized mainly in the cylindrical part of the channel and in the plume, which suggests that the thruster should suffer lower erosion of the channel walls due to fast ion bombardment. Plasma density has a maximum of about $(2.6–3.8)\times10^{12}\,\mathrm{cm}^{-3}$ at the thruster axis. At the discharge voltage of 300 V, the maximum electron temperature is about 21 eV, which is not enough to produce multiple ionization in the accelerated flux of Xe^+ ions. © *2004 American Institute of Physics.* [DOI: 10.1063/1.1642734]

I. INTRODUCTION

Scaling to low power Hall thrusters requires a thruster channel size to be decreased while the magnetic field must be increased inversely to the scaling factor.[1] Implementation of the latter requirement is technically challenging because of magnetic saturation in the miniaturized inner parts of the magnetic core. A linear scaling down of the magnetic circuit leaves almost no room for magnetic poles or for heat shields, making difficult the achievement of the optimal magnetic fields. Nonoptimal magnetic fields result in enhanced power and ion losses, heating, and erosion of the thruster parts, particularly the critical inner parts of the coaxial channel and magnetic circuit. Thruster channel erosion due to fast ion bombardment is one of the main factors limiting the lifetime of Hall thrusters.[1] Thus, to avoid enhanced channel erosion is one of the major challenges for low-power Hall thruster technology.

Currently existing low-power Hall thruster laboratory prototypes with channel diameters 2–4 cm operate at 100–300 W power levels with efficiencies in the range of 10%–30%.[2–4] However, further scaling of the conventional geometry Hall thruster down to subcentimeter size[5] results in even lower efficiencies (6% at power level of about 100 W). The low efficiency might arise from a large axial electron current, enhanced by magnetic field degradation due to excessive heating of the thruster magnets, or from a low degree of propellant ionization. Thus, miniaturizing the conventional annular Hall thruster does not appear to be straightforward.

A cylindrical Hall thruster (CHT), suggested in Ref. 6, is illustrated in Fig. 1(a). The thruster consists of a boron–nitride ceramic channel, an annular anode, which serves also as a gas distributor, two electromagnetic coils, and a magnetic core. What distinguishes this thruster from conventional annular and end-Hall thrusters[7] is the cylindrical configuration with an enhanced radial component of the cusp-type magnetic field. The magnetic field lines intersect the ceramic channel walls. The electron drifts are closed, with the magnetic field lines forming equipotential surfaces, with $E=-\nu_e\times B$. Ion thrust is generated by the axial component of the Lorentz force, proportional to the radial magnetic field and the azimuthal electron current.

The cylindrical channel features a short annular region and a longer cylindrical region. The length of the annular region is selected to be approximately equal to an ionization mean free path of a neutral atom. This provides high ionization of the working gas at the boundary of the annular and the cylindrical regions. In this case, most of the voltage drop occurs in the cylindrical region. It may be possible to accelerate ions in the cylindrical channel predominantly in the longitudinal direction and towards the thruster axis, thus reducing the channel wall wear.

Compared to a conventional geometry (annular) Hall thruster, the CHT has lower surface-to-volume ratio and, therefore, potentially smaller wall losses in the channel. Having potentially smaller wall losses in the channel, a CHT should suffer lower erosion and heating of the thruster parts, particularly the critical inner parts of the channel and magnetic circuit. This makes the concept of a CHT very promising for low-power applications.

A relatively large 9 cm diam version of a cylindrical thruster exhibited performance comparable with conventional annular Hall thrusters in the subkilowatt power range.[6] It was shown that the ion acceleration in the 9 cm CHT occurs in the cylindrical part of the channel. A miniature 2.6 cm diam CHT, in the power range 50–300 W, was shown to have efficiency (15%–32%) and thrust (2.5–12 mN) similar to those of the annular thruster of the same size.[8] It was found that both the 9 and 2.6 cm CHTs have unusually high propellant ionization efficiency, compared to conventional

[a]Author to whom correspondence should be addressed; electronic mail: asmirnov@pppl.gov

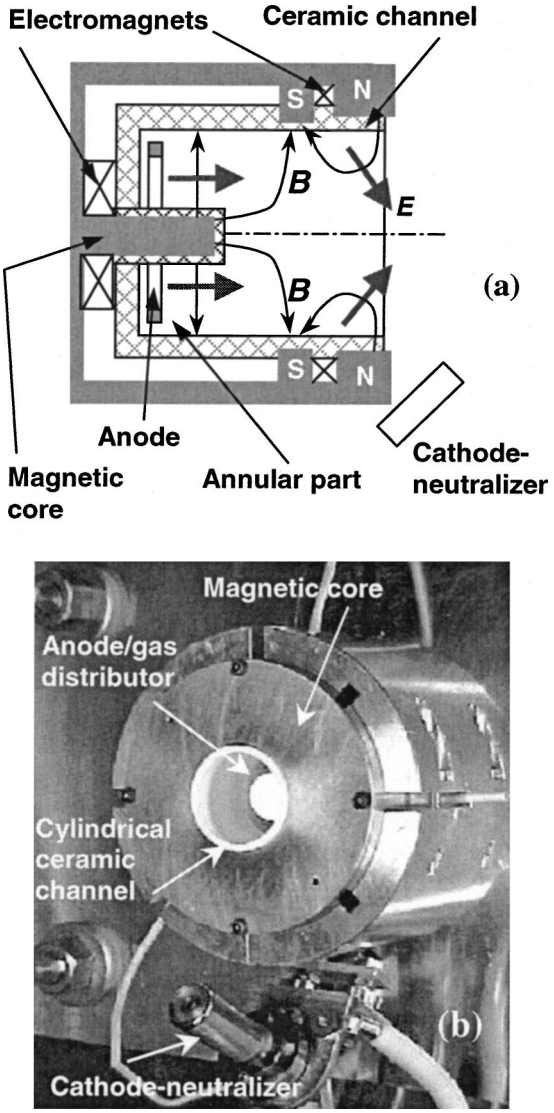

FIG. 1. (a) Schematic of a cylindrical Hall thruster and (b) the 2.6 cm cylindrical Hall thruster.

Hall thrusters. The ratio of the total ion current to the effective propellant mass flow current, in the case of the 2.6 cm CHT, could exceed unity, which clearly indicates the presence of multicharged Xe ions in the ion flux generated by the thruster. In a recent work,[9] numerical simulations, performed within the framework of a quasi-one-dimensional (1D) stationary thruster model, showed that space-charge saturation of a wall sheath limits the temperature of Maxwellian electrons in the thruster at the value insufficient for strong ionization and multicharged ions generation. Therefore, the increase in the propellant utilization in the 2.6 cm CHT does not appear to be quantitatively explained by a reduction of plasma wall losses.

In the present work, distribution of plasma potential ϕ_{pl} and plasma (ion) density N_i inside the 2.6 cm CHT was studied by means of stationary and slow movable floating emissive and biased Langmuir probes. We emphasize that these measurements of plasma parameters were performed in a Hall thruster of a very low power ($\sim$100 W). It was found that even though the radial component of the magnetic field has a maximum inside the annular part of the CHT, the larger fraction of the applied voltage, as in the 9 cm CHT, is localized in the cylindrical region. A significant potential drop was observed also in the plume, where the magnetic field is much weaker than in conventional Hall thrusters. At the discharge voltage of 300 V, the maximum electron temperature was about 21 eV, which is not enough to produce multiple ionization in the accelerated flux of Xe^+ ions. Distribution of plasma density in the cylindrical part of the channel appeared to be very nonuniform in the radial direction: N_i peaked at the thruster axis at about $(2.6–3.8)\times10^{12}\,\mathrm{cm}^{-3}$, while near the outer wall N_i was on the order of $(1.5–6)\times10^{11}\,\mathrm{cm}^{-3}$.

This article is organized as follows: In Sec. II, the experimental setup is described and considerations of probe design are given. Section III describes the experimental procedure. The key results obtained in the experiments are presented, and their implications are discussed in Sec. IV. In Sec. V, we summarize our main conclusions.

II. EXPERIMENTAL SETUP

A. Thruster and vacuum facility

The 2.6 cm CHT, shown in Fig. 1(b), was scaled down from the 9 cm CHT to operate at about 200 W power level. The total length of the channel is 2.2 cm, and the annular region is approximately 0.6 cm long. The outer and the inner diameters of the channel are 2.6 and 1.4 cm, respectively. The overall diameter and the thruster length are both 7 cm. The magnetic circuit consists of two coils connected to separate power supplies. The currents in the coils are counterdirected to produce a cusp magnetic field with a strong radial component in the channel.

Magnetic field profiles in the 2.6 cm CHT are shown in Fig. 2(a). The radial component B_r of the magnetic field reaches its maximum a few millimeters from the anode and then reduces towards the channel exit. Although the axial component B_z is also strong, the magnetic field in the annular part of the channel is predominantly radial, the average angle between the field line and the normal to the walls is about 30° [see Fig. 2(b)]. The magnetic field has a mirror-type structure near the thruster axis, with the maximum $B \sim 1400\,\mathrm{G}$ at the central ceramic piece wall.

Implementation of internal probe diagnostics in the 2.6 cm CHT presented a very challenging technical task because of a very compact thruster design. In order to accommodate the probes, several modifications of the original magnetic circuit were made. The changes in the magnetic circuit were designed so that the magnetic field inside the channel remained unperturbed. This fact was carefully checked by both magnetic field measurements and simulations.

The experiments took place in a 0.4 m^3 vacuum chamber, equipped with a turbomolecular pumping system (Small Hall Thruster facility at Princeton Plasma Physics Laboratory). The measured pumping speed reached $\sim1200\pm200$ l/s for Xe. The working background pressure of Xe was about 6.5×10^{-5} Torr for the total propellant flow rate of 0.6 mg/s. Two commercial flow controllers, 0–10 and 0–15 sccm, volumetrically calibrated in the flow rate range of 1–10

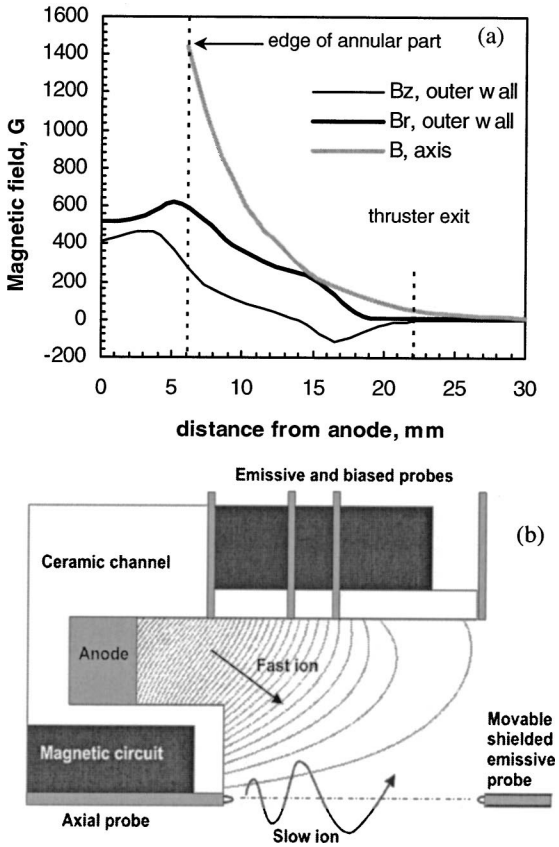

FIG. 2. (a) Magnetic field profiles in the 2.6 cm CHT: $I_{back}=2.5$ A, $I_{front}=-1$ A and (b) probe setup used in the experiments. Magnetic field distribution is given for the same coil currents as in (a). Fast and slow ion trajectories are also indicated.

sccm, supplied research grade Xe gas to the anode and the cathode, respectively.

A commercial HeatWave plasma source was used as a cathode neutralizer. The cathode was mounted so that the angle between the thruster and cathode axes was 30° [see Fig. 1(b)]. The cathode outlet orifice was located approximately 54 mm away radially and 20 mm downstream from the center of the channel exit. The cathode flow rate of Xe was held at 0.2 mg/s for all the experiments.

B. Probe design considerations

The harsh environment of a Hall thruster creates significant difficulties in collection and interpretation of Langmuir probe data. Probe diagnostics is complicated due to the presence of streaming ions, electron fluxes, high electric, and magnetic fields. However, despite these complications, Langmuir probes remain the simplest and cheapest diagnostic tool for plasma measurements inside a Hall thruster. Both stationary[10–12] and movable[6,13–16] probes were successfully used for plasma measurements in kilowatt and subkilowatt Hall thrusters.

Hall thruster plasma is extremely sensitive to probe immersion. Probe-induced perturbations of the discharge in kilowatt Hall thrusters are typically very strong: The discharge current jumps to 150%–200% of its unperturbed value.[14,15] However, in Hall thrusters with outer channel diameters of 12–17 cm, the discharge current perturbations can be decreased by the use of a fast reciprocating probe[15,16] and almost eliminated if the fast probe of a special design is used.[17]

The use of complex and expensive fast probe positioning setup did not seem reasonable for the purposes of the present preliminary study. It was also doubtful whether the fast probe immersion diagnostics, even if implemented, can be effectively used for a very small size plasma discharge studied in the present work. Therefore, we chose to use stationary probes mounted on the outer channel wall to measure plasma parameters inside the thruster. Typically, such probes do not induce significant perturbations in a Hall thruster discharge.[10–12] Deducing bulk plasma properties from the near-wall measurements is complicated due to sheath and presheath phenomena. This question was not addressed in the present work. Plasma parameters measured at the wall are understood as quantities averaged over the length of the flux tube sampled by a probe.

High magnetic field in the 2.6 cm CHT complicates probe measurements dramatically. For the unmagnetized probe theory to be valid for a cylindrical probe oriented perpendicular to the magnetic field, the probe diameter d must be smaller than the electron gyrodiameter[18]

$$d \ll \frac{4.8[T_e(\mathrm{eV})]^{1/2}}{B(\mathrm{G})}. \tag{1}$$

For the measurements on the outer channel wall of the 2.6 cm CHT ($T_e \sim 14-20$ eV), the most severe limitation is imposed on a probe in the annular part of the channel, where the maximum B is about 750 G: $d<0.24$ mm. Such thin probes, if used for biased measurements to determine plasma potential, appear to be impractical because of their short lifetime limited due to fast ion bombardment. More importantly, probe erosion changes the length of the wire that collects plasma. Thus, a large uncertainty in the probe collection area can be introduced.

From the above considerations, the floating emissive probe technique[19] was chosen for the plasma potential measurements in the 2.6 cm CHT. The floating emissive probe provides a direct instantaneous measure of the plasma potential regardless of whether the plasma is stationary or flowing. No voltage sweep is required. Emission of electrons from a hot floating filament into plasma tends to eliminate the potential difference between the probe and the plasma. However, the space charge of cold emitted electrons ($T_e^{\mathrm{em}} \ll T_e^{\mathrm{plasma}}$) causes saturation of the sheath surrounding the hot filament, and floating potential of the emissive probe ϕ_f^{em} occurs to be downshifted from the plasma potential ϕ_{pl} by a value on the order of the plasma electron temperature T_e[20,21]

$$\Delta\phi = \phi_{\mathrm{pl}} - \phi_f^{\mathrm{em}} \approx 1.5 T_e. \tag{2}$$

In magnetized plasmas the emitted electrons tend to follow the magnetic field rather than expanding away from the probe in all directions. Thus, the magnetic field lines should intersect the probe wire, and condition (1) should be satisfied for the wire diameter.

Due to their large mass, ions in a Hall thruster are not magnetized, $r_{iL} \gg L$, where r_{iL} is the ion gyroradius and L is

the characteristic channel size. In principle, plasma (ion) density N_i can be conveniently derived from the ion saturation current I_{is} measured by a probe. In the 2.6 cm CHT, planar probes mounted flush with the outer channel wall were used to measure I_{is}. The same planar probes were also employed for floating potential measurements. To have a supplemental independent check of the plasma potential, the planar probes were used as well for biased measurements in the regime of electron collection. For the conditions in the 2.6 cm CHT, no significant reduction of the electron saturation current on a planar probe is expected (see Sec. III). However, strong magnetic and electric fields and fast ions cause rounding of the knee of the probe current–voltage ($I-V$) characteristic.

It is well known that a Hall thruster operation is strongly influenced by the channel wall material. For example, by placing conductive or emissive segmented electrodes along a ceramic wall it is possible to control the distribution of electric field in the thruster plasma.[22,23] In the present experiments, several flush-mounted probes had to be used simultaneously to measure axial profiles and to study azimuthal symmetry of the discharge. Taking into account the small channel size of the thruster, it was necessary to minimize the probe diameter in order not to change the regime of thruster operation.

C. Probe setup

Probe setup used in the experiments is shown in Fig. 2(b). Measurements along the outer channel wall were performed at four axial locations: $z=5$, 10.3, 13.5, and 22 mm. Distance was measured from the anode towards the thruster exit. Four radially inserted probes were used at each axial location. The probes were distributed azimuthally at 90° to each other to monitor azimuthal symmetry of the discharge. Typically, one emissive and three cold planar probes were used at each axial location.

The emitting portion of an emissive probe was a loop-shaped filament made of 0.1 mm diam thoriated tungsten wire. Thus, condition (1) was satisfied, at least marginally, everywhere in the channel. The ends of the filament were inserted down a double bore alumina tubing (outer diameter 1.22 mm) along with copper wire leads. The width and height of the emissive loop protruding into the plasma was approximately 1 mm. The probes were mounted so that the end of the alumina insulator was flush with the channel wall and the loop plane was parallel to the anode surface. Due to the small emissive wire diameter, the lifetime of the emissive probes was very short and the probes had to be replaced frequently.

The planar probes were constructed of 0.74 mm diam tungsten wire and 1.22 mm outer diam alumina tubing. The collecting surface of the wire was flush with the edge of the alumina insulator and with the channel wall.

An additional slow movable emissive probe was used to determine plasma potential at the thruster exit plane and in the plume. The use of a special probe shield, developed in Ref. 17, allowed us to minimize probe-induced perturbations of the discharge. The probe was mounted on a shaft that could be moved by hand in radial and axial directions. Yet another probe, which we call an axial probe, was inserted through a small orifice in the magnetic pole to measure plasma parameters near the wall of the central ceramic piece [see Fig. 2(b)]. Details of the probes operation and data analysis techniques are discussed in Sec. III.

III. EXPERIMENTAL PROCEDURE

In the present study the 2.6 cm CHT was operated at the discharge voltages of 250–300 V and Xe flow rate of 0.4 mg/s. The input power ranged from 140 to 180 W. Stability of the thruster operation was strongly influenced by the cathode neutralizer. The cathode ability to sustain the discharge in the self-heating mode declined in time, possibly due to emissive filament contamination by the sputtered probe material. Therefore, to achieve stable thruster operation, it was necessary to operate the cathode in the so-called outgas mode, when a heating current of about 10 A was supplied to the filament.

Emissive probes were dc current heated. Probe heating power was about 20 W. Heating current and voltage were monitored with multimeters. Floating potentials of cold and emissive probes as well as the cathode potential were measured relative to the ground by a PC-based data acquisition system. 50 MΩ: 0.5 MΩ low-inductance dividers and isolation amplifiers with high input impedances were used for these measurements.

In the biased probe measurements typical bias voltage was varied between $-10T_e$ and $+2T_e$ (relative to the plasma potential) with a ~20 s sweep. Probe bias voltage and collected current were recorded by the data acquisition system.

To avoid influence of the probes on the thruster operation, measurements at only two axial locations were done simultaneously: While data were gathered at one axial position, measurements at the other position provided reference data for a cross check between different runs. Only one emissive probe was operated during each experiment. No perturbations of the discharge due to the electron emission from the probe were observed. To check repeatability of the results, measurements at each axial location were performed 2–3 times with different (emissive and biased) probes in most of the operating regimes.

The procedure to determine plasma potential and the electron temperature was as follows. After thruster startup, once the steady-state operation was achieved (typically, in 15–20 min), an emissive probe was heated to emit electrons. The heating current was increased until the floating potential of the probe reached a nearly saturated value. Then, floating potentials ϕ_f^{em} and ϕ_f^c of the hot emissive probe and three cold planar probes at the same axial location were measured. (In the case of measurements with the axial probe and the movable probe in the plume, floating potentials ϕ_f^c and ϕ_f^{em} were determined sequentially with the same probe, first cold, then heated.) The uncertainty of ϕ_f^{em} saturation was found to be ± 2 V. Estimated voltage drop along the hot emissive filament was ~0.5 V. Measurements of floating potentials on the outer channel wall showed that the discharge in the 2.6 cm

CHT could be azimuthally asymmetric. At a given axial location, values of ϕ_f^c measured by different probes could vary from each other by about 30% of their amplitude. However, in most of the regimes this deviation was less than 10%. The value of the floating potential, averaged over three planar probes, $\phi_f^{\mathrm{av}}=\langle\phi_f^c\rangle$, was used in data analysis to characterize the plasma at each axial location.

In Xe plasma with the Maxwellian electron distribution function (EDF), the floating potential ϕ_f is related to the plasma potential ϕ_{pl} as[24]

$$\phi_f=\phi_{\mathrm{pl}}-5.77T_e. \tag{3}$$

Combining this formula with Eq. (2), we find that the electron temperature and plasma potential can be deduced from the measured quantities as

$$T_e=(\phi_f^{\mathrm{em}}-\phi_f^{\mathrm{av}})/4.27, \tag{4}$$

$$\phi_{\mathrm{pl}}=\phi_f^{\mathrm{em}}+1.5T_e, \tag{5}$$

We emphasize the fact that Eqs. (4)–(5) are valid only for the Maxwellian EDF. In a Hall thruster, the EDF can be non-Maxwellian due to the presence of the strong magnetic field and electron $E\times B$ drift. Along with it, electron–wall collisions can depopulate the tail of the EDF,[25] thus strongly reducing the effective secondary electron emission from the channel walls and changing the overall balance of the electron energy.[9] Although some observations demonstrated that the EDF in the 2.6 cm CHT is indeed non-Maxwellian, thorough investigation of the EDF, which presents an overwhelmingly complicated experimental problem, was not attempted in the present work. For a non-Maxwellian EDF quantity T_e, calculated from Eq. (4), is believed to give a rough estimate of the mean electron energy. A similar approach to estimation of T_e, applied to a larger Hall thruster,[26] produced values of electron energy that agreed well with other measurements.[27] The overall uncertainty associated with determination of ϕ_{pl} and T_e according to Eqs. (4)–(5) is difficult to quantify because of: (i) herein mentioned azimuthal asymmetry of the discharge in the 2.6 cm CHT and (ii) possibly non-Maxwellian EDF.

To check the values of plasma potential and electron temperature obtained with emissive probes, the standard biased Langmuir probe technique[24] was employed. The magnetic field in the 2.6 cm CHT is not expected to significantly decrease the electron saturation current I_{es} collected by the 0.74 mm diam planar probe. A depletion of the electron density in the magnetic flux tube sampled by a probe occurs when the rate of electron diffusion across the magnetic field becomes much less than the rate of electron escape to the probe along the field lines[28]

$$\frac{16D_\perp}{d^2}\ll\frac{\nu_{\mathrm{te}}}{L_{\mathrm{coll}}}.$$

Here, $D_\perp$ is the coefficient of diffusion across the magnetic field, d is the probe diameter, ν_{te} is the electron thermal velocity, and L_{coll} is the collection length of the flux tube, which is determined by the distance between the thruster walls. If combined with the expression for $D_\perp$ in a strong magnetic field, $D_\perp=v_e(\nu_{\mathrm{te}}/\omega_{\mathrm{ce}})^2$, the last inequality can be recast in terms of the electron collision frequency v_e

$$v_e\ll\frac{d^2\omega_{\mathrm{ce}}^2}{16\nu_{\mathrm{te}}L_{\mathrm{coll}}}, \tag{6}$$

Here, ω_{ce} is the electron cyclotron frequency. It is generally accepted that three mechanisms contribute to the total electron collision frequency v_e in a Hall thruster: (i) the classical electron–neutral collisions; (ii) the anomalous Bohm diffusion; and (iii) the electron–wall collisions (scattering and secondary electron emission). We can estimate the corresponding collision frequencies as follows. In the annular part of the 2.6 cm CHT at Xe flow of 0.4 mg/s the maximum neutral atom density N_n is about $4\times10^{13}\,\mathrm{cm}^{-3}$. The typical T_e is about 16 eV. Therefore, the maximum electron–neutral collision frequency $v_{\mathrm{en}}\sim\sigma_{\mathrm{en}}N_n\nu_{\mathrm{te}}$($\sigma_{\mathrm{en}}\sim4\times10^{-15}\,\mathrm{cm}^2$ is the total electron scattering cross section for Xe) does not exceed approximately $3\times10^7\,\mathrm{s}^{-1}$. The frequency of anomalous Bohm diffusion is proportional to the electron gyrofrequency: $v_a\sim\alpha\omega_{\mathrm{ce}}$. Both 1D and 2D Hall thruster models[29,30] show that the best agreement between the experimental and simulated data is achieved when α is chosen to be a few times (typically, 5–6) smaller than Bohm's coefficient 1/16. Assuming $\alpha\sim10^{-2}$ we find that in the annular part of the 2.6 cm CHT v_a should be about $1.5\times10^8\,\mathrm{s}^{-1}$. The maximum possible electron–wall collision frequency[1] v_{ew} is on the order of $\nu_{\mathrm{te}}/L_{\mathrm{coll}}\sim2.5\times10^8\,\mathrm{s}^{-1}$. Therefore, we conclude that the electron conductivity is expected to be due mainly to electron–wall collisions and to electron scattering in the field fluctuations. The total electron collision frequency v_e is about $4\times10^8\,\mathrm{s}^{-1}$, while the right-hand side of Eq. (6) is approximately equal to $6.5\times10^8\,\mathrm{s}^{-1}$. According to Ref. 28, v_e must be more than 1 order of magnitude smaller than the right-hand side of Eq. (6) to get at least a twofold reduction of the electron saturation current on a probe. Thus, under conditions of the present experiment the electron saturation current is not expected to decrease significantly, as compared with an unmagnetized plasma case.

Typical electron branch of the probe $I-V$ characteristic is shown in Fig. 3(a). From the semilog graph of the probe $I-V$ trace, ϕ_{pl} was determined at the extrapolated knee, and T_e was estimated as $T_e=(\phi_{\mathrm{pl}}-\phi_f^{\mathrm{av}})/5.77$. In most of the measurements, despite the knee rounding, it was possible to unambiguously fit the trace with the straight lines just above and below the plasma potential. The physical uncertainty of the plasma potential measurement by a biased probe was estimated to be ±10 V. However, in the measurements at the channel exit ($z=22$ mm location, outer wall) the knee of the probe traces appeared to be completely smoothed out, possibly due to fast ions collection. Thus, comparison of emissive and biased probe data was carried out for probes located at $z=5$, 10.3, and 13.5 mm only.

The $I-V$ trace can be seen to deviate appreciably from a straight line at the bias voltages ~40 V below the plasma potential. Although this might be due to the non-Maxwellian shape of the EDF, it is hard to assert so with confidence because many factors can cause distortion of the trace. Among those are high magnetic field, sheath, and edge ef-

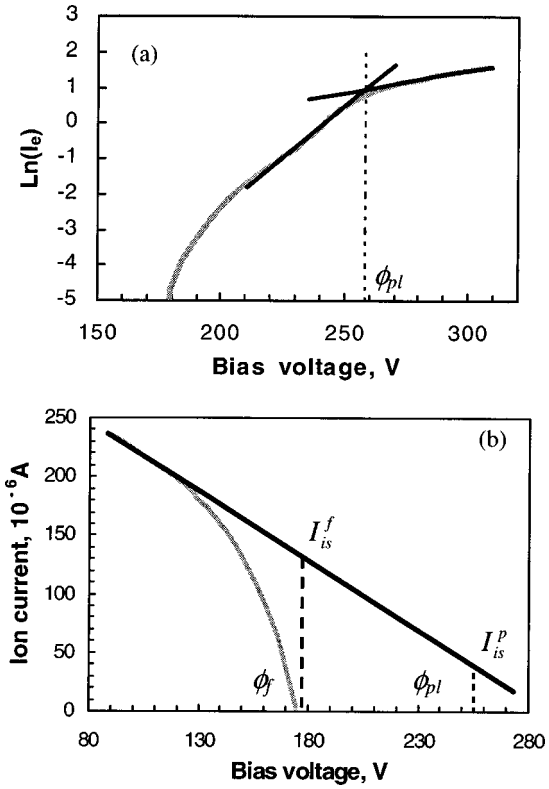

FIG. 3. (a) Typical $\ln(I_e)$ vs bias voltage trace and (b) determination of I_{is}^{f} and I_{is}^{p} based on linear extrapolation of the ion current to the floating and the plasma potentials.

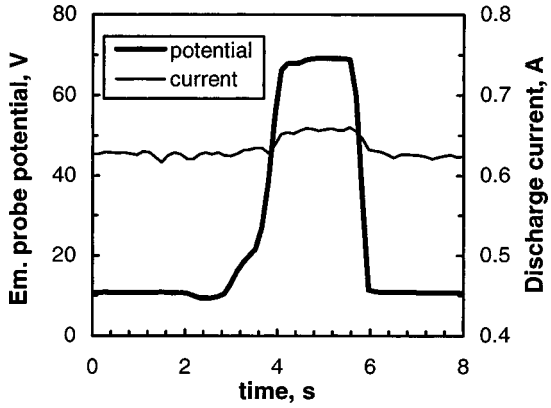

FIG. 4. Perturbation of the discharge current induced by the shielded emissive probe. The emissive filament is at the center of the channel exit cross section. Heating current was turned on at $t \approx 2$ s, gradually increased until the probe floating potential saturated at $t \approx 4.8$ s, and turned off at $t \approx 5.6$ s.

fects at the probe mounted flush with the ceramic wall, and collection of fast ions. It is worth mentioning that the values of T_e deduced from the slope of the linear part of the probe $I-V$ trace, $T_e \approx e[d(\mathrm{Ln}(I_e))/dV]^{-1}$, could exceed those obtained from Eq. (4) by factor of about 1.5–2. However, the systematic study of different electron populations in the 2.6 cm CHT did not seem feasible with the present probe setup.

Measurements of the ion saturation current I_{is} showed that the plasma density N_i in the 2.6 cm CHT ranged over $(1-10)\times 10^{11}\,\mathrm{cm}^{-3}$. (Plasma is assumed to be quasineutral, thus, we do not distinguish between the electron and ion densities.) Typical T_e was about 16 eV. Then, the Debye length λ_D and sheath thickness s at negative bias potential $\sim -10\,T_e$ become $\lambda_D \approx (3-9)\times 10^{-2}$ mm and $s \approx (1.7-5)\times 10^{-1}$ mm. Therefore, for the 0.74 mm diam planar probe, collection area variation due to the edge effects and sheath expansion should be significant. It must be noted here that in a thruster channel with diameter $D = 26$ mm strong sheath expansion effects are virtually inevitable for a planar probe of any reasonably small size $d \ll D$. As shown in Fig. 3(b), the ion branch of a typical probe $I-V$ characteristic does not saturate indeed. It is customary to overcome this current nonsaturation by linearly extrapolating the ion current, measured at highly negative bias voltages, to give the expected saturation current I_{is}^{p} at the plasma potential. However, sheath expansion can be nonlinear.[31] In fact, we found that the values of I_{is}^{p} tend to underestimate the real ion saturation current: The measured ratio $I_{\mathrm{es}}/I_{\mathrm{is}}^{p}$ appears to be larger than the value predicted by the unmagnetized probe theory, $1.64\sqrt{M_i/2\pi m_e} \sim 320$ for Xe plasma. On the other hand, the values of I_{is}^{f}, obtained from linear extrapolation of the ion current to the floating potential, appear to be closer to the expected ion saturation current (see discussion in Sec. IV C). N_i was estimated using Bohm's approximation[24]

$$I_{\mathrm{is}} = 0.61 N_i e A_p \sqrt{\frac{T_e}{M_i}}. \tag{7}$$

Here, A_p is the physical probe area, M_i is the mass of a Xe atom, and e is the electron charge. Ions are assumed to be singly charged. To characterize uncertainty in the determination of N_i, the upper and the lower bounds for N_i were calculated from the measured values of I_{is}^{f} and I_{is}^{p}, respectively.

Measurements of the plasma potential at the thruster axis appeared to be extremely difficult to perform, primarily because of a very short lifetime of emissive probes in the dense near-axis plasma with fast ions. Once heated to emit electrons, the emissive filament was destroyed in approximately 40–50 s at the channel exit, and in less than 2 s inside the thruster.

Probe insertion in the 2.6 cm CHT induced fierce discharge perturbations if no precautions were taken. For example, if a 1.22 mm diam alumina tube, emulating the probe, was inserted axially a few millimeters inside the cylindrical part of the channel, the mean discharge current increased by a factor of ~2. The use of a molybdenum shield that covered the entire lateral surface of the probe[17] allowed us to reduce the perturbations significantly. When the tip of the emissive probe was at the thruster exit, the average increase in the discharge current was on the order of 10% (see Fig. 4).

IV. EXPERIMENTAL RESULTS AND DISCUSSION

The results presented in this section were obtained for the magnetic field distribution shown in Fig. 2. Currents in the back and front thruster coils were held constant at 2.5 and −1 A, respectively. The cathode neutralizer was operated in the outgas mode, unless specified otherwise.

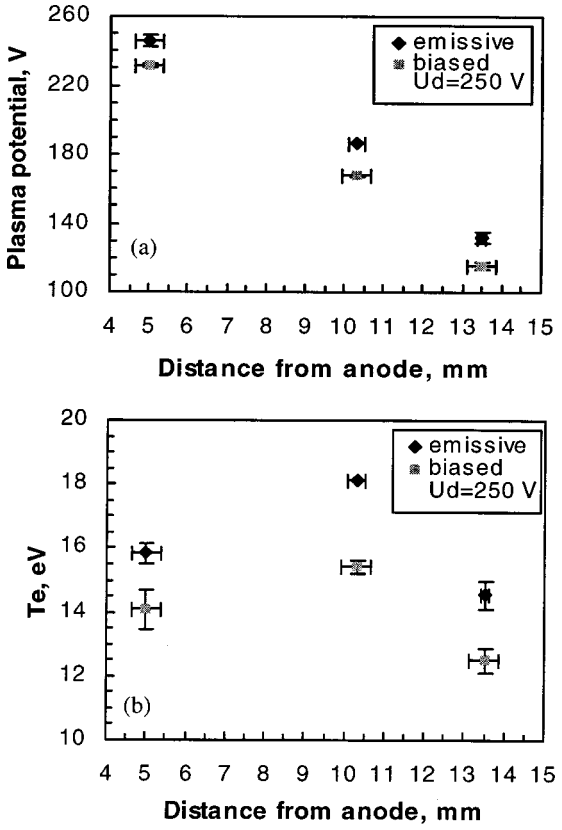

FIG. 5. (a) Plasma potential relative to the cathode and (b) electron temperature profiles measured by emissive and biased probes at the outer channel wall: $U_d = 250$ V. Axial probes locations are $z = 5$, 10.3, and 13.5 mm. The edge of the annular part and the channel exit are located at $z = 6$ and 22 mm, respectively. *Y*-axis error bars represent the entire statistical spread of the measured data. *X*-axis error bars show the maximum width of the magnetic flux tube sampled by a probe.

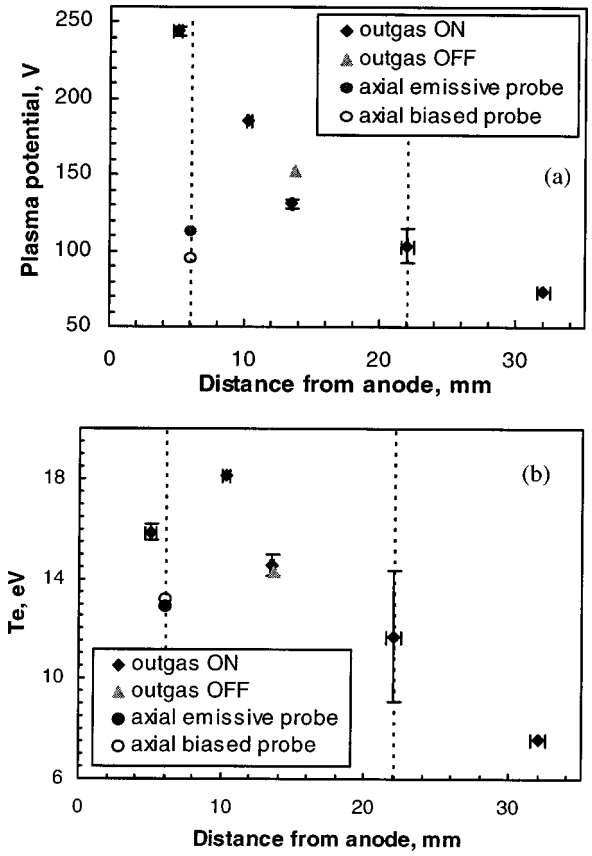

FIG. 6. (a) Plasma potential relative to the cathode and (b) the electron temperature measured by emissive probes at the outer wall ($z = 5$, 10.3, and 13.5 mm) and at the thruster axis ($z = 22$ and 32 mm): $U_d = 250$ V. The values of ϕ_{pl} and T_e, measured at the central ceramic piece wall by the axial probe, are also shown. Dashed lines at $z = 6$ and 22 mm show the edge of the annular part and the channel exit, respectively.

A. Comparison of the results of emissive and biased probe measurements

Typical profiles of ϕ_{pl} and T_e, measured by emissive and biased probes at the outer channel wall, are shown in Fig. 5. Repeatability of the results is indicated by *y*-axis error bars. (Throughout this section, where available, the entire statistical spread of the measured data is represented by *y*-axis error bars.) *X*-axis error bars show the maximum width of the magnetic flux tube sampled by a probe.

As follows from the graphs, the values of ϕ_{pl} and T_e measured with biased probes are somewhat smaller than those measured with emissive probes. However, the maximum deviation between the results, which is about 16%, is believed to be within the uncertainties for both measurement methods.

All the results presented below were obtained with the use of the emissive probe technique.

B. Plasma potential and electron temperature

Measurements performed by the shielded emissive probe showed that radial variation of ϕ_{pl} and T_e at the channel exit and in the near plume was weak. Therefore, data measured at the thruster axis ($z = 22$ and 32 mm) and at the outer channel wall ($z = 5$, 10.3, and 13.5 mm) was combined to get the axial profiles of plasma potential and estimated electron temperature given in Fig. 6.

As follows from Fig. 6, the potential drop in the 2.6 cm CHT is localized mainly in the cylindrical part of the channel and beyond the thruster exit, in the plume. Ionization of neutrals occurs at the boundary of annular and cylindrical parts of the channel because at $z = 5$ mm the electrons have already enough energy to ionize Xe atoms.

Since equipotentials tend to follow the magnetic field lines, a complex 2D structure of the accelerating electric field is formed in the 2.6 cm CHT. As indicated in Fig. 3(b), ions born in the annular part of the channel should be accelerated predominantly in the *z* direction and towards the thruster axis. Therefore, the outer wall erosion might be decreased and a longer lifetime of the cylindrical thruster, as compared with conventional geometry Hall thrusters, could be expected.

Some of the ions born in the annular part of the channel hit the central ceramic piece on their way out of the thruster. The probe at $z = 10.3$ mm location on the outer wall samples the magnetic flux tube that intersects the central ceramic wall near the edge of the annular part of the channel. The expected potential drop along the inner channel wall is then approximately equal to or less than 60 V. The fraction of

accelerated ions that actually hit the wall is not large because the central pole is relatively short. Therefore, erosion rate of the central ceramic piece in the 2.6 cm CHT should not be significant.

Surprisingly, a considerable potential drop was observed along the thruster axis in the plume, where the magnetic field, as opposed to conventional (annular) Hall thrusters, is weak. High potential drop could, in principle, appear if the plume was not completely neutralized by the cathode. At $z = 92$ mm (not shown in Fig. 6) plasma potentials relative to the cathode and the electron temperature at the thruster axis were about 44 V and 2.7 eV, respectively. Switching the cathode from the outgas mode to the self-heating mode caused a slight downstream shift of the acceleration region and did not significantly change the electron temperature. The influence of the cathode on the electron dynamics and ion acceleration in the Hall thruster plume is worth studying further.

As can be seen in Fig. 6(a), the potential drop along the thruster axis between the central ceramic piece and the channel exit is insignificant. Its maximum possible value is within the data spread of the present measurements, which is about 25 V. Much larger potential drops along the magnetic field lines were observed in the Kaufman ion source,[7] which has a mirror-type magnetic field distribution similar to that in the central part of the CHT. In Ref. 7, the potential drop was found to scale as $\Delta\phi \sim T_e \ln(R)/e$, where R is the mirror ratio of the magnetic plug. Physical mechanisms underlying the equalizing of the plasma potential along the magnetic mirror plug in the 2.6 cm CHT are the subject of ongoing research.

Variation of ϕ_{pl} and T_e profiles inside the thruster with discharge voltage is illustrated by graphs given in Fig. 7. Measurements at $U_d = 275$ V, $z = 13.5$ mm, and at $U_d = 300$ V, $z = 5$, and 13.5 mm were performed with the cathode operated in the self-heating mode. Potential profiles rise gradually with U_d while remaining similar to each other. The maximum estimated electron temperature is about 21 eV, which is too low to produce multiple ionization in the accelerated flux of Xe^+ ions. This result agrees with the conclusion made in a recent theoretical work.[9] Numerical simulations, performed within the framework of a quasi-1D stationary thruster model, showed that space-charge saturation of a wall sheath limits the temperature of Maxwellian electrons in the thruster at a value insufficient for strong ionization and multicharged ions generation. Therefore, the increase in the propellant utilization in the 2.6 cm CHT does not appear to be quantitatively explained by a reduction of plasma wall losses.

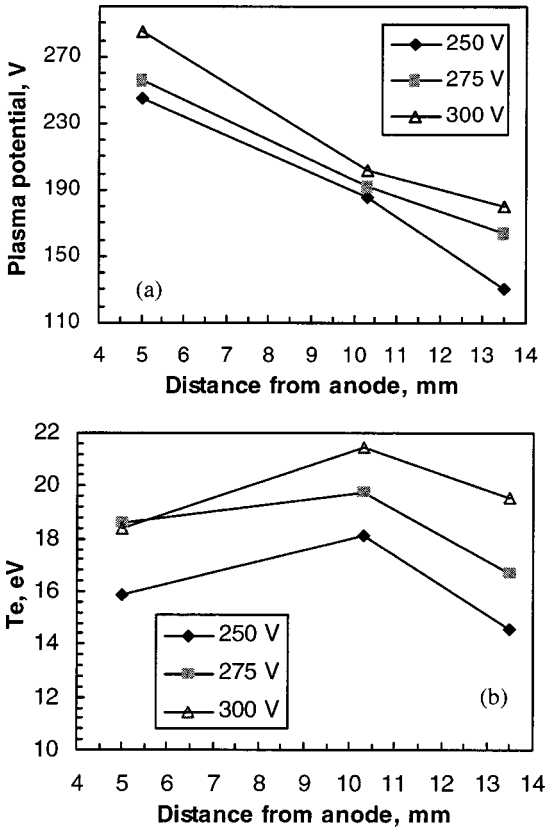

FIG. 7. Variation of the (a) plasma potential relative to the cathode and (b) electron temperature profiles inside the thruster with discharge voltage, as measured by emissive probes at the outer channel wall. The edge of the annular part and the channel exit are located at $z = 6$ and 22 mm, respectively.

C. Plasma density

The upper and the lower bounds of N_i, measured at the outer channel wall as well as at the central ceramic piece wall, are shown in Fig. 8. Due to the focusing electric field in the cylindrical channel, contribution of fast ions to the ion saturation current measured at $z = 5$ and 13.5 mm axial locations is expected to be negligible. Therefore, calculation of N_i from Eq. (7) should be accurate enough. Higher values of N_i, obtained at $z = 22$ mm, may be due to the fact that the probe at the channel exit could intercept some fast ions. In this case Eq. (7) leads to overestimation of N_i. Fast ions impinging the outer wall at the channel exit might appear, for example, because of the overfocusing of the ion flux. A considerable flexibility in the magnetic configuration of the 2.6

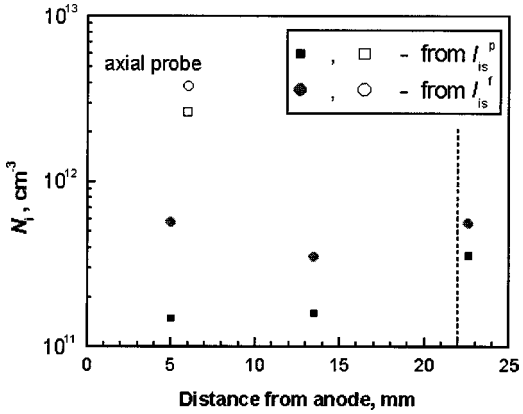

FIG. 8. The upper (circles) and the lower (squares) bounds of N_i, determined from the measured values of I_{is}^{f} and I_{is}^{p}, respectively. Ud=250 V measurements were performed at the outer channel wall at $z = 5$, 13.5, and 22.5 mm locations (solid symbols) and at the central ceramic piece wall at the thruster axis ($z = 6$ mm, open symbols). Dashed line at $z = 22$ mm shows the location of the thruster exit plane.

cm CHT might allow one to control the direction of ion acceleration and eliminate the overfocusing, if it in fact occurs.

The magnetic field in the annular part of the 2.6 cm CHT is mainly radial. Using the estimates of the electron collision frequencies ν_a and ν_{ew} obtained in Sec. III, we can determine the plasma density necessary to conduct the observed electric current across the magnetic field in the annular part of the channel. First we exploit Ohm's law to find the average electron velocity in the axial direction U_e[29,30]

$$\frac{m_e N_e U_e \omega_{ce}^2}{\nu_e} = eN_e\left(E - \frac{1}{eN_e}\frac{d(N_e T_e)}{dz}\right). \tag{8}$$

Here, E is the electric field and z is the axial coordinate. The pressure term in the parentheses can be neglected because near the boundary of the annular and the cylindrical regions E is on the order of 120 V/cm [see Fig. 6(a)], while the product $N_e T_e$ does not vary much [see Figs. 6(b) and 8]. Thus, $U_e \sim eE\nu_e/m_e\omega_{ce}^2 \sim 3.8\times 10^5$ cm/s. The potential drop $\Delta\phi$ from the anode up to the $z=5$ mm location is about 10 V. The fraction of multicharged Xe ions in the total ion flux in the annular part of the channel is expected to be small because of the relatively low T_e. Therefore, the maximum ion axial fluid velocity $U_i = (2e\Delta\phi/M_i)^{0.5}$ is approximately equal to 3.8×10^5 cm/s. In order to estimate N_e we employ the current continuity

$$I = eS_a(U_i + U_e)N_e, \tag{9}$$

where I is the total electric current, which is equal to 0.6 A at $U_d = 250$ V, and $S_a = 3.77$ cm^2 is the anode area. Substituting all the numerical values into Eq. (9), we get $N_e \sim 1.3\times 10^{12}$ cm^{-3}. Thus, the estimated plasma density in the annular part of the channel appears to be closer to the upper bound for N_i, obtained from extrapolation of the measured ion current to the floating potential.

It is important to note that the plasma density has a prominent peak at the thruster axis: N_i at the axis is 4–8 times larger than in the annular part of the channel. The deviation between the upper and the lower estimates of N_i at the axis is, on the other hand, rather small, about 30% of the mean value of N_i. This implies that the sheath expansion effect plays a less important role for the axial probe due to higher plasma density. The sharp maximum in N_i might be a manifestation of the convergent ion flux.

One can speculate that high propellant utilization in the CHT is explained by an enhanced ionization in the central near-axis part of the discharge. Since the axial magnetic field lines appear to be almost equipotential, ions born in the plasma at the thruster axis will make a few radial bounces before leaving the channel, as sketched in Fig. 2(b). Therefore, the ion residence time in a very high-density near-axis plasma may be increased. This, in conjunction with the fact that the electrons streaming into the thruster from the cathode can have a substantial high-energy population,[32] might bring about multiple ionization of Xe atoms.

V. CONCLUSIONS

Conventional (annular) Hall thrusters become inefficient when scaled to small sizes because of the large surface-to-volume ratio and the difficulty in miniaturizing the magnetic circuit. Along with it, erosion of the walls of a small annular channel can severely limit the thruster lifetime. An alternative approach, which may be more suitable for scaling to low power, is a cylindrical Hall thruster. Both the 9 cm CHT, operated in the subkilowatt power range, and the miniature 2.6 cm CHT, operated in the power range 50–300 W, exhibit performance comparable with conventional annular Hall thrusters of similar size.

Plasma potential, electron temperature, and plasma (ion) density profiles inside the 2.6 cm CHT were measured using stationary and slow movable emissive and biased Langmuir probes. Even though the radial component of the magnetic field has a maximum inside the annular part of the 2.6 cm CHT, the potential drop is localized mainly in the cylindrical part of the channel and in the plume. Ion acceleration is expected to occur predominantly in the longitudinal direction and towards the thruster axis. Therefore, the CHT, having lower surface-to-volume ratio as compared with conventional Hall thrusters, should suffer lower erosion of the channel walls due to fast ion bombardment.

A considerable potential drop along the thruster axis in the plume, where the magnetic field of the 2.6 cm CHT, as opposed to conventional (annular) Hall thrusters, is weak, might be due to an incomplete neutralization of the plume plasma by the cathode. The influence of the cathode on the electron dynamics and ion acceleration in the Hall thruster plume is a subject of ongoing research.

The distribution of plasma density in the cylindrical part of the channel appears to be very nonuniform in the radial direction: The density peaks at the thruster axis at about $(2.6–3.8)\times 10^{12}$ cm^{-3}, while near the outer wall at the edge of the annular and the cylindrical parts of the channel it is on the order of $(1.5–6)\times 10^{11}$ cm^{-3}.

The axial profile of the estimated electron temperature in the 2.6 cm CHT is rather flat. At the discharge voltage of 300 V, the maximum electron temperature is about 21 eV, which is not enough to produce multiple ionization in the accelerated flux of Xe^+ ions. Therefore, the increase in the propellant utilization in the 2.6 cm CHT does not appear to be explained solely by a reduction of plasma wall losses. It is suggested that formation of multicharged Xe ions might be possible in the dense near-axis plasma, where the residence time of slow ions can be increased by the electrostatic trapping in the radial direction.

ACKNOWLEDGMENTS

The authors wish to thank David Staack and Leonid Dorf for their help with the experiments and useful discussions and comments on this article. This work was supported by grants from AFOSR, DARPA, and U.S. DOE Contract No. AC02-76CH0-3073.

[1] A. I. Morozov and V. V. Savelyev, in *Review of Plasma Physics*, edited by B. B. Kadomtsev and V. D. Shafranov (Consultants Bureau, New York, 2000), Vol. 21, p. 203.
[2] V. Hruby, J. Monheiser, B. Pote, C. Freeman, and W. Connolly, in *Proceedings of the 26th International Electric Propulsion Conference, Kitakyushu, Japan* (Electric Rocket Propulsion Society, Cleveland, OH, 1999), IEPC 99-092.
[3] D. Jacobson and R. Jankovsky, in *Proceedings of the 34th Joint Propulsion Conference, Cleveland, Ohio* (American Institute of Aeronautics and Astronautics, Reston, VA, 1998), AIAA 98-3792.
[4] O. Gorshkov, in *Proceedings of the 34th Joint Propulsion Conference, Cleveland, Ohio* (American Institute of Aeronautics and Astronautics, Reston, VA, 1998), AIAA 98-3929.
[5] V. Khayms and M. Martinez-Sanches, in *Micropropulsion for Small Spacecraft, Progress in Astronautics and Aeronautics*, edited by M. M. Micci and A. D. Ketsdever (American Institute of Aeronautics and Astronautics, Reston, VA, 2000), Vol. 187, p. 45.
[6] Y. Raitses and N. J. Fisch, Phys. Plasmas **8**, 2579 (2001).
[7] H. R. Kaufman, R. S. Robinson, and R. I. Seddon, J. Vac. Sci. Technol. A **5**, 2081 (1987).
[8] A. Smirnov, Y. Raitses, and N. J. Fisch, J. Appl. Phys. **92**, 5673 (2002).
[9] A. Smirnov, Y. Raitses, and N. J. Fisch, J. Appl. Phys. **94**, 852 (2003).
[10] A. I. Bugrova, A. I. Morozov, and V. K. Kharchevnikov, Sov. Phys. Tech. Phys. **30**, 613 (1985).
[11] A. I. Bugrova, A. V. Desyatskov, and A. I. Morozov, Sov. J. Plasma Phys. **18**, 501 (1992).
[12] G. Guerrini, C. Michaut, M. Bacal, A. N. Vesselovzorov, and A. A. Pogorelov, Rev. Sci. Instrum. **69**, 804 (1998).
[13] A. I. Morozov, Yu. V. Esinchuk, G. N. Tilinin, A. V. Trofimov, Yu. A. Sharov, and G. Ya. Shchepkin, Sov. Phys. Tech. Phys. **17**, 38 (1972).
[14] W. A. Hargus, Jr. and M. A. Capelli, *Proceedings of the 35th Joint Propulsion Conference, Los Angeles, CA* (American Institute of Aeronautics and Astronautics, Reston, VA, 1999), AIAA 99-2721.
[15] J. M. Haas and A. D. Gallimore, *Proceedings of the 26th International Electric Propulsion Conference, Kitakyushu, Japan* (Electric Rocket Propulsion Society, Cleveland, OH, 1999), IEPC 99-078.
[16] Y. Raitses, D. Staack, A. Dunaevsky, L. Dorf, and N. J. Fisch, *Proceedings of the 28th International Electric Propulsion Conference, Toulouse, France* (Electric Rocket Propulsion Society, Cleveland, OH, 2003), IEPC 03-0139.
[17] D. Staack, Y. Raitses, and N. J. Fisch, Rev. Sci. Instrum. (accepted for publication).
[18] Yu. M. Kagan and V. I. Perel, Sov. Phys. Tech. Phys. **13**, 1348 (1969).
[19] N. Hershkowitz, *Plasma Diagnostics: Discharge Parameters and Chemistry* (Academic, New York, 1989), pp. 146–152.
[20] G. D. Hobbs and J. A. Wesson, Plasma Phys. **9**, 85 (1967).
[21] L. A. Schwager, Phys. Fluids B **5**, 631 (1993).
[22] Y. Raitses, L. A. Dorf, A. A. Litvak, and N. J. Fisch, J. Appl. Phys. **88**, 1263 (2000).
[23] D. Staack, Y. Raitses, and N. J. Fisch, *Proceedings of the 28th International Electric Propulsion Conference, Toulouse, France* (Electric Rocket Propulsion Society, Cleveland, OH, 2003), IEPC 03-0273.
[24] J. D. Swift and M. J. R. Schwar, *Electrostatic Probes For Plasma Diagnostics* (Elsevier, New York, 1969).
[25] I. Kaganovich, M. Misina, S. V. Berezhnoi, and R. Gijbels, Phys. Rev. E **61**, 1875 (2000).
[26] N. B. Meezan, W. A. Hargus, and M. A. Cappelli, Phys. Rev. E **63**, 026410 (2001).
[27] M. Bishaev and V. Kim, Sov. Phys. Tech. Phys. **23**, 1055 (1978).
[28] B.-W. Koo, N. Hershkowitz, and M. Sarfaty, J. Appl. Phys. **86**, 1213 (1999).
[29] E. Ahedo, J. M. Gallardo, and M. Martinez-Sanchez, in *Proceedings of the 38th Joint Propulsion Conference, Indianapolis, IN* (American Institute of Aeronautics and Astronautics, Reston, VA, 2002), AIAA 02-4244.
[30] M. Keidar, I. D. Boyd, and I. I. Beilis, Phys. Plasmas **8**, 5315 (2001).
[31] M. B. Hopkins and W. G. Graham, Rev. Sci. Instrum. **57**, 2210 (1986).
[32] V. Yu. Fedotov, A. A. Ivanov, G. Guerrini, A. N. Vesselovzorov, and M. Bacal, Phys. Plasmas **6**, 4360 (1999).